IEEE Access
Multidisciplinary ⋮ Rapid Review ⋮ Open Access Journal

Received 10 March 2024, accepted 3 April 2024, date of publication 8 April 2024, date of current version 15 April 2024.

*Digital Object Identifier 10.1109/ACCESS.2024.3385779*

RESEARCH ARTICLE

# MonoBot: A Single-Actuator Walking Robot

**URIYA LAX, ODED MEDINA, AND NIR SHVALB**
Department of Mechanical Engineering, Ariel University, Ariel 4070000, Israel
Corresponding author: Nir Shvalb (nirsh@ariel.ac.il)

**ABSTRACT** This paper introduces the design and analysis of novel planar mobile robot operated by a single actuator. Distinct from conventional multi-actuator designs, this robot achieves both walking and turning motions through a single actuator mechanism, thereby simplifying construction and control. The design focuses on mechanical and electronic minimalism and efficiency. We formulate the governing dynamic equations using Euler-Lagrange formalism by which we optimize the robot's design. The study concludes with a series of experiments that demonstrate the robot's translation and rotation.

**INDEX TERMS** Mobile robot, walking robot, single actuator, dynamic analysis, Euler-Lagrange equations.

## I. INTRODUCTION

In the realm of robotics, the method of actuation is a key factor that defines a robot's capabilities. Robotic arms and manifolds [1], are equipped with actuators at each joint for precise control. Overactuated robots, which possess more actuators than joints, offer enhanced adaptability and control precision [2], whereas underactuated robots, characterized by having fewer actuators than joints, face control complexities but gain advantages from their simple design. In the context of very large swarms, the simplicity of each individual agent becomes imperative to maintain cost-effectiveness [3].

### A. BACKGROUND

Under-actuated mechanisms have emerged as an increasingly important area of research in robotics, as evidenced by studies like Collins et al. [4], Lai et al. [5], and McMahon et al. [6]. Unlike fully-actuated systems, which use motors or other actuators to control every joint and degree of freedom, under-actuated systems utilize fewer actuators and depend on passive dynamics for motion generation, as discussed in Aoustin and Formalskii [7] and Bellicoso et al. [8]. This approach, inspired by natural locomotion in animals and humans, emphasizes the body's mechanical properties and environmental interactions in motion generation [9]. Under-actuated mechanisms potentially offer greater efficiency, robustness, and adaptability than fully-actuated systems, but they also present significant control, stability, and design challenges.

The associate editor coordinating the review of this manuscript and approving it for publication was Agustin Leobardo Herrera-May.

It is widely recognized that traversing a plane requires at least two degrees of freedom, applicable to both walking robots and wheeled platforms. For instance, *Omni-wheeled platforms* need at least three actuators; *Ackermann steering platforms*, common in vehicles, require two actuators; and *Differential steering (skid) platforms* also demand two actuators, one for each side of the platform.

Common under-actuated walking robots in literature can generally be classified into two categories:

*Passive dynamic walkers*, which rely on gravity and their mechanical properties to generate a walking gait. The design and control principles of these walkers are well-established, as seen in examples like the rimless wheel walker [10] and the compass gait walker [11]. *Compliant walkers*, which incorporate compliant elements in their legs for energy storage and release during walking. These robots typically have two or more actuators to control the timing and amplitude of leg movements, exemplified by the *tensegrity* robot [12] and the quadruped robot [13].

### B. SINGLE ACTUATED MOBILE-ROBOTS

Over recent years, sparse research has considered the design of a planar agent with only a single actuator. In this regard, one should mention the well-known single-actuator walking robot designed by the coupling of two linkage mechanisms, as presented in Zhang and Arakelian [14].

Zarouk and Fearing [15] introduced a remarkable single-actuator robot capable of moving straight, turning clockwise, or counterclockwise. This is achieved by alternating the acceleration of three legs in contact with the ground, enabling precise rotations.

**TABLE 1.** A comparison with previous research in under-actuated planar robots.

| Publication | Actuation type | Mechanism | Forward traversing method | Turning method |
|---|---|---|---|---|
| [14] Zhang et al. | Single motor | Pantograph and a cam mechanism | Turning the motor (crank-rocker mechanism) | N/A |
| [15] Zarrouk et al. | Single DC motor | Worm gear and gears concatenation | Turning the motor | Accelerating and decelerating the legs rotation |
| [16] Ito et al. | Single DC motor | Caster-wheeled platform with momentum rod | Sinusoidal motor rotation | Asymmetrical sinusoidal motor rotation |
| [17] Hariri et al. | Piezoelectric actuator | Vibrations using three mechanical modes | Mode 1 vibration | Mode 2 or 3 vibration |
| [18] Hoover et al. | Single DC motor and two SMA wires | Spatial linkage | Turning the motor (crank-rocker mechanism) | Changing leg stiffness using active SMA wires |
| MonoBot | Single DC motor | A single omni-wheel | Sinusoidal motor rotation | Asymmetrical sinusoidal motor rotation or Constant motor rotation |

The researchers in Ito et al. [16] presented a novel mechanism for a caster-wheeled robot with a single actuator. Utilizing a sinusoidal rotor rotation, the robot can move forward, and by adding an offset to the actuator's signal, a curved motion path is achieved.

Hariri et al. [17] introduced a highly maneuverable, under-actuated, legged piezoelectric miniature robot. It comprises a piezoelectric actuator bonded onto a thin diamond-shaped aluminum plate with three rigidly attached legs. Different standing wave vibration modes of the thin plate enable three distinct motions: forward, clockwise rotation, and anticlockwise rotation.

Inspired by cockroaches, Hoover et al. [18] designed an under-actuated, small-sized hexapod robot. It measures $10cm$ in length, weighs $24grams$, and is capable of running at 14 times its body length per second, and performing dynamic turning maneuvers. These maneuvers are made possible by altering the stiffness of the legs on one side of the robot.

Lastly, the single-actuated mobile robot presented in Böhm and Zimmermann [19] is designed as a tensegrity structure and can translate through uniaxial bidirectional actuation.

### C. MOTIVATION AND CONTRIBUTION

Here we introduce the "MonoBot" - a single DOF walking robot that can traverse the plane by translation and rotation applying an approach that stands out for its simplicity. The main idea is harnessing a single actuator and leveraging the robot's nonlinear dynamics. Our design offers an elegant and efficient solution both in mechanical and electronic designs. Table 1 offers a detailed comparison between our work and prior studies in the realm of under-actuated planar robots. The design introduced here:

1) Unlike others, it is capable of rotating on its own axis as well as turning in any radius of curvature.
2) Has a single moving part (and so is [17]; but unlike all others: 4 in [16], 5 in [18], 8 in [14] and 12 in [15]).
3) Can carry payloads of up to 5 times its own weight, as reported in [17] (compared with 2 in [18])
4) Low power consumption of $0.64W$ which only underperformes $0.178W$ in [15] (compared with $3.2W$ in [17], $20W$ in [14]).
   But
5) The MonoBot's striding speed is low. Provided in body lengths per second it is 0.3 compared with 0.3 in [16]; 2 in [15]; 4 in [14]; and both [17] [18] with 14.

We believe that multi-robot system research (such as swarm robots) may benefit from our simple mechanical and electrical design.

### D. PAPER ORGANIZATION

This paper is organized as follows: Section II introduces the mechanical model. Section III introduces the associated dynamic model which we used to optimize our mechanism. Section IV-A presents the set of simulated and real-world experiments demonstrating the robot's capabilities. Section VI concludes the paper.

## II. MECHANICAL DESIGN

The design of the robot emphasizes simplicity in both mechanical and electronic aspects. The mechanical design and code are available in the supplementary materials of this paper.

### A. GENERAL SPECIFICATIONS

"The MonoBot has a weight of 107 grams, measures $70mm$ in length, $65mm$ in width, and has a height of $50mm$. It is powered by a single N20 Gear DC Motor, which drives an omni-wheel. The motor is controlled by an ESP-01 Wi-Fi ESP8266 module, a cost-effective micro-controller with Wi-Fi capability and two GPIO pins, in conjunction with a $DRV8838$ DC motor driver. Power is supplied by a single 18650 lithium-ion rechargeable battery, providing $3.7V$,

sufficient for approximately 30 minutes of continuous operation. The electrical Printed Circuit Board (PCB) serves as the MonoBot's body, hosting the electrical circuit and connections for all components. Additionally, two front leg extensions are attached to the PCB, providing stability to the mechanism and also functioning as terminals for the battery charger.

### B. OPERATION PRINCIPLE

Applying current to the motor results in the wheel turning in a specific direction, thereby generating momentum on the MonoBot's body. This momentum causes the body to turn in the opposite direction. Consequently, one of the legs lifts off the ground while the robot balances on the other leg, forming a pivot point. This results in a rotational movement where the wheel continues to turn until the other leg makes contact with the ground again. Similarly, applying current in the reverse direction causes the opposite leg to become the pivotal axis of rotation. By rapidly turning the wheel from side to side for brief durations ($\leq 100ms$), a zigzag movement is achieved that closely approximates a forward motion (Figure 1). By adjusting the rotation periods of the wheel on each angular direction, one can create circular or curved movements at will, up to a pure rotation. This is demonstrated in the videos showcasing the robot in action [20] or in video.

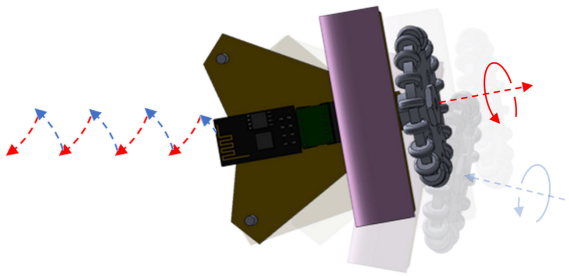

**FIGURE 1.** A linear translation by utilizing a zigzag walking movement.

## III. DYNAMIC ANALYSIS

A dynamic model has been developed by formulating Euler-Lagrange equations, based on the assumption that at any given moment, one of the robot's legs is in contact with the ground. This model effectively captures the system's dynamics, offering valuable insights into the robot's behavior and aiding in the analysis and development of control strategies.

### A. PRELIMINARIES

Accordingly, we set the origin of the main coordinate system at that contact point, and denote its origin by $O$. The $z$-axis is set to be perpendicular to the ground, and the $y$-axis is directed towards the initial point of contact of the second leg with the ground (see Figure 4). We denote the MonoBot's body angular velocity about the $\widehat{b}$ axis by $\dot{\theta}_b$ where $\vec{b}$ is the vector pointing from the origin $O$ to the center of the wheel and $\widehat{b}$ the corresponding unit vector.

| Symbol | Definition |
|---|---|
| $O$ | The origin of the axis system x-y-z |
| $\widehat{b}$ | An axis from the origin to the center of the wheel (direction vector) |
| $\widehat{w}$ | The motor axis (direction vector) |
| $\dot{\theta}_b$ | The MonoBot angular velocity around axis $\widehat{b}$ |
| $\dot{\theta}_w$ | The MonoBot angular velocity around axis $\widehat{w}$ |
| $\dot{\theta}_z$ | The MonoBot angular velocity around axis $\widehat{z}$ |
| $\vec{b}$ | Vector from the origin $O$ to the wheel's center of mass |
| $r$ | The radius of the wheel |
| $\vec{r}_0$ | Vector from the origin $O$ to the MonoBot's center of mass |
| $h$ | The MonoBot length |
| $\ell$ | The distance between the leg and the wheel in the MonoBots main plane |
| $\alpha$ | the angle between $\ell$ and $h$ |
| $R_z$ | Rotation matrix about the $\widehat{z}$ axis |
| $R_b$ | Rotation matrix about the $\widehat{b}$ axis |
| $R$ | The MonoBot rotation matrix |
| $\vec{\Omega}_b$ | The angular velocity of the MonoBot's body about the origin $O$ |
| $\vec{\Omega}_w$ | The wheel's angular velocity around its center of mass |
| $K$ | Cross product in matrix form |
| $\vec{v}_w$ | Wheel's linear velocity |
| $I_O$ | The body's moment of inertia relation to the origin $O$ |
| $I_w$ | The wheel's moment of inertia calculated at its center of mass |
| $m$ | The mass of the MonoBot |
| $m_w$ | The mass of the wheel |
| $E_k$ | The kinetic energy of the MonoBot |
| $E_p$ | The robot's potential energy |

$\dot{\theta}_z$ denotes the MonoBot's angular velocity about the $z$ axis. We distinguish between the motor's angular velocity (given in the robot's coordinate system) and that of the wheel (given in world coordinates). Accordingly, the motor's angular velocity is denoted by $-\dot{\theta}_w$ about its axis $\widehat{w}$.

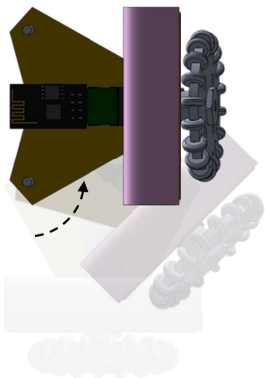

**FIGURE 2.** Continuously activating the wheel in the desired direction results with rotation about one of the legs.

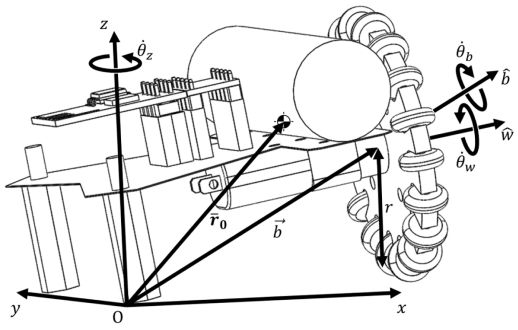


**FIGURE 3.** The coordinate system and the rotation velocities.

Throughout the movement, the mechanism rotates about $\widehat{b}$ and about $\widehat{z}$. The combined rotation matrix $R = R_b R_z$, is defined such that $R_b$ is the rotation matrix about the current $\widehat{b}$ axis and $R_z$ is the rotation matrix about the $\widehat{z}$ axis, that is:

$$R_z = \begin{bmatrix} c_z & -s_z & 0 \\ s_z & c_z & 0 \\ 0 & 0 & 1 \end{bmatrix} \tag{1}$$

$$R_b = \begin{bmatrix} c_b + b_x^2\gamma_b & b_x b_y \gamma_b - b_z s_b & b_x b_z \gamma_b + b_y s_b \\ b_x b_y \gamma_b + b_z s_b & c_b + b_y^2 \gamma_b & b_y b_z \gamma_b - b_x s_b \\ b_x b_z \gamma_b - b_y s_b & b_y b_z \gamma_b + b_x s_b & c_b + b_z^2 \gamma_b \end{bmatrix} \tag{2}$$

where $c_b$, $s_b$ and $\gamma_b$ denotes $\cos(\theta_b)$, $\sin(\theta_b)$ and $1 - \cos(\theta_b)$ respectively. Following the above definitions, the rotation axis of the body $\widehat{b}$ is obtained by $\widehat{b} = R\widehat{b}_0$, where $\widehat{b}_0$ is the rotation axis of the body at the initial state, before the movement starts and $R = R_b R_z$. Similarly, the rotation unit axis of the wheel $\widehat{w}$ is obtained by $\widehat{w} = R\widehat{w}_0$, where $\widehat{w}_0$ is the direction of the wheel's axis at the initial state.

### B. ANGULAR VELOCITIES

For brevity, we mark $\vec{\Omega}_b$ to be the angular velocity of the robot's body about the origin $O$. That is, the sum of the angular velocities $\dot{\theta}_z$ about $\widehat{z}$ together with the angular velocity $\dot{\theta}_b$ about $\widehat{b}$. The approximated (magnitude of the) angular velocity $\dot{\theta}_z$ as a function of $\dot{\theta}_w$ is given by:

$$\dot{\theta}_z = -\frac{r(\dot{\theta}_w - \dot{\theta}_b \widehat{b}_0^\top \widehat{w}_0)\sin(\alpha)}{\ell} = -\frac{hr}{\ell^2}(\dot{\theta}_w - \dot{\theta}_b \widehat{b}_0^\top \widehat{w}_0) \tag{3}$$

where $r$ is the radius of the wheel, $h$ is the central axis length of the mechanism and $\ell$ is the horizontal distance from the pivot leg to the center of the wheel. The first term on the RHS of the Eq. 3 is evident from Figure 4 while the second term acounts for the robots rotation about $\vec{b}$.

The angular velocity vector of the robot's body is therefore:

$$\vec{\Omega}_b = R_z \widehat{b}_0 \dot{\theta}_b + \widehat{z}\dot{\theta}_z = R_z \widehat{b}_0 \dot{\theta}_b - \widehat{z}\dot{\theta}_w \frac{hr}{\ell^2} \tag{4}$$

The wheel's angular velocity vector $\vec{\Omega}_w$ is the rotation velocity $\widehat{b}\dot{\theta}_b$ of the robot together with the rotation velocity around the motor axis given as a vector $\widehat{w}\dot{\theta}_w$:

$$\vec{\Omega}_w = \widehat{w}_0 \dot{\theta}_w + \widehat{b}_0 \dot{\theta}_b \tag{5}$$

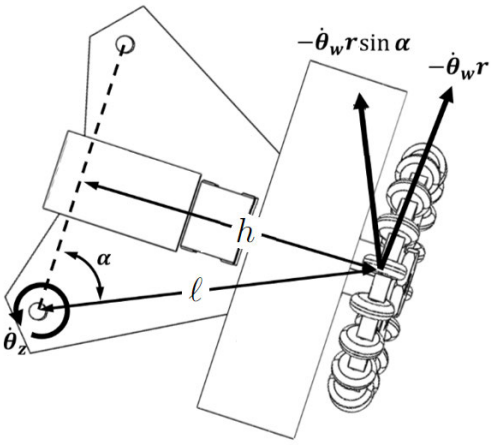


**FIGURE 4.** The approximated angular velocity $\dot{\theta}_z$ as a function of $\dot{\theta}_w$.

The rotation velocity $\widehat{z}\dot{\theta}_z$ of the robot adds to the wheel a linear velocity $\vec{v}_w$. The cross product can be equivalently written as matrix multiplication:

$$\begin{aligned} \vec{v}_w &= \widehat{z}\dot{\theta}_z \times R_z \vec{b} \\ &= -\widehat{z}\dot{\theta}_w \frac{hr}{\ell^2} \times R_z \vec{b} \\ &= \dot{\theta}_w \begin{bmatrix} 0 & \frac{hr}{\ell^2} & 0 \\ -\frac{hr}{\ell^2} & 0 & 0 \\ 0 & 0 & 0 \end{bmatrix} R_z \vec{b} \\ &= \dot{\theta}_w K R_z \vec{b} \end{aligned} \tag{6}$$

where $K$ is the RHS matrix expression.

### C. KINETIC AND POTENTIAL ENERGIES

We mark the wheel's moment of inertia calculated at its center of mass in the trivial coordinate system by $I_w$. We use the notation $I_O$ for the inertia tensor of the robot's body with respect to the system of axes whose origin is $O$. We denote the inertia tensor of the robot's body with respect to its center of mass by $I_c$. To complete this, that moments of inertia transforms as $R^\top I R$ in a rotating axis system. Furthermore, recall that the kinetic energy of a rigid body in a system of axes whose origin is point $O$, where $O$ is a stationary point, is $\frac{1}{2}\omega^\top I_O \omega$ while the kinetic energy of a rigid body when a system of axes is located at the center of mass is given by $E_k = \frac{1}{2} m v_c^\top v_c + \frac{1}{2}\omega^\top I_c \omega$.

The sum of the energies of the robot's body due to its rotational movement $\vec{\Omega}_b$ around the point $O$ and that of the wheel energy due to its rotational $\vec{\Omega}_w$ and linear $\vec{v}_w$ movement of its center of mass is:

$$E_k = \frac{1}{2}\vec{\Omega}_b^\top R^\top I_O R \vec{\Omega}_b + \frac{1}{2} m_w \vec{v}_w^\top \vec{v}_w + \frac{1}{2}\vec{\Omega}_w^\top I_w \vec{\Omega}_w \tag{7}$$

which after tedious development, which is provided in the Appendix, takes the form:

$$E_k = \frac{1}{2}\dot{\theta}_b^2 I_1 + \dot{\theta}_b \dot{\theta}_w I_2 + \frac{1}{2}\dot{\theta}_w^2 I_3 \tag{8}$$

where:

$$I_1 = \widehat{b}_0^\top R_z^\top R^\top I_O R R_z \widehat{b}_0 + \widehat{b}_0^\top I_w \widehat{b}_0$$
$$I_2 = \widehat{b}_0^\top I_w \widehat{w}_0 - \frac{hr}{\ell^2}\widehat{z}^\top R^\top I_O R R_z \widehat{b}_0$$
$$I_3 = \frac{h^2 r^2}{\ell^4}\widehat{z}^\top R^\top I_O R \widehat{z} + m_w \vec{b}^\top R_z^\top K^\top K R_z \vec{b} + \widehat{w}_0^\top I_w \widehat{w}_0$$

When the robot is at rest on the ground, its potential energy is set to zero. We denote $r_0$ as the vector extending from the origin $O$ to the center of mass of the MonoBot, as illustrated in Figure 4. The MonoBot's mass is represented by $m$. With these definitions, the potential energy due to gravity is given by:

$$E_p = \widehat{z}^\top (R\vec{r}_0 - \vec{r}_0) mg \tag{9}$$

Which is proportional to the height difference of the center of mass from the ground between the initial position (when both feet are on the ground) and the position after the rotation movement.

### D. EQUATIONS OF MOTION

Defining $\mathcal{L} = E_k - E_p$ and substituting the above to the Euler-Lagrange equations $\frac{d}{dt}\left(\frac{\partial \mathcal{L}}{\partial \dot{\theta}_i}\right) - \frac{\partial \mathcal{L}}{\partial \theta_i} = Q_i$ and solve in the $\theta_b$ coordinate the MonoBot's motion equations take the explicit form:

$$\ddot{\theta}_b I_1 + \ddot{\theta}_w I_2 + \dot{\theta}_b^2 \frac{1}{2}\left(\frac{\partial I_1}{\partial \theta_b}\right) + \dot{\theta}_w^2 \left(\frac{\partial I_2}{\partial \theta_w} - \frac{1}{2}\frac{\partial I_3}{\partial \theta_b}\right) + \dot{\theta}_b \dot{\theta}_w \left(\frac{\partial I_1}{\partial \theta_w}\right) + \frac{\partial E_p}{\partial \theta_b} = Q_b \tag{10}$$

Note that in the coordinate $\widehat{b}$ there is no external moment, therefore $Q_b = 0$. Equation 10 and the rotation in the $z$ direction given by Equation 3 constitutes the dynamics of the robot which is governed by $\theta_w, \dot{\theta}_w, \ddot{\theta}_w$ and $\theta_b, \dot{\theta}_b, \ddot{\theta}_b$.

## IV. EXPERIMENTATION

The set of motion equations 3,10 are obviously too intricate to be solved analytically. We therefore, resort to a numerical study.

The motion equations indicate that four controllables that govern the movement of the robot: The moments of inertia $I_w$ and $I_O$ (by design); the wheel acceleration $\ddot{\theta}_w$ (via controller); and the maximum wheel angular velocity $\dot{\theta}_w$ (actuator choice). A dynamic analysis for the robot may examine the effect of each.

### A. NUMERICAL STUDY

One can therefore formulate a single numerical step, from which we can project the entire movement of the robot by calculating $\dot{\theta}_b = \dot{\theta}_b + \ddot{\theta}_b \Delta t$ and $\dot{\theta}_w = \dot{\theta}_w + \ddot{\theta}_w \Delta t$ followed by $\theta_b = \theta_b + \dot{\theta}_b \Delta t + \frac{1}{2}\ddot{\theta}_b \Delta t^2$ and $\theta_w = \theta_w + \dot{\theta}_w \cdot dt + \frac{1}{2}\ddot{\theta}_w \Delta t^2$.

Initially, the velocities and angles are set to zero. We set $\Delta t$ to 0.01ms and the wheel acceleration $\ddot{\theta}_w$ is given as DC motor acceleration step response. The body acceleration $\ddot{\theta}_b$ is extracted using the equation of motion 10 above. This simulates the single step. But note that this will not do. This is so since the robot initiates its motion with smaller steps and assumes a steady state behaviour only after several steps.

In Eq. 10, we present a formalism that specifically applies to the scenario where one leg is anchored and the other is in motion, corresponding to a half step period. To accurately represent the continuous walking motion, we employ a mirrored version of this formalism. This involves swapping the roles of the left and right legs, while maintaining the same underlying assumptions. The initial conditions for each new gait cycle are set as the final generalized velocities from the preceding cycle.

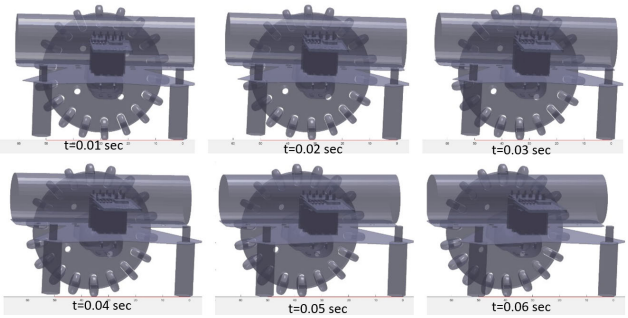


**FIGURE 5. A front view of the simulated single step (compare with Figure 6).**

### B. REAL WORLD TESTS

The simulated model (Figures 7 and 5) was initially validated using a real experiment, showcasing a compelling resemblance between the two.

A set of 50 experimenters were conducted. In each experiment the robot (Section II above) was set to travel in a straight line of length $1m$ on a flat surface. A typical experiment is presented in Figures 6 and 8. The robot average speed was measured to be 0.3 body lengths per second. A second set of 50 experiments demonstrated that the rotational angular velocity of the robot was measured to be $2\pi/5$ rad/sec.

We tested the capabilities of the robot in handling additional weight while maintaining motion. The robot itself weighs 60 grams, while the 18650 LiPo cell it utilizes, adds 50 grams to its total weight. Our experiments revealed that the robot can effectively carry an additional weight of up to 250 grams without impeding its motion. This amounts to approximately 5 times its own net weight.

To investigate the impact of wheel acceleration on translation, a series of simulated experiments were conducted using MATLAB platform. The robot's positions were calculated at regular intervals throughout the experiment to observe the effects of different wheel accelerations. The wheel's acceleration $\ddot{\theta}_w$ values was varied in the range $2\pi/0.001$ to $2\pi/0.1$ per squared second.

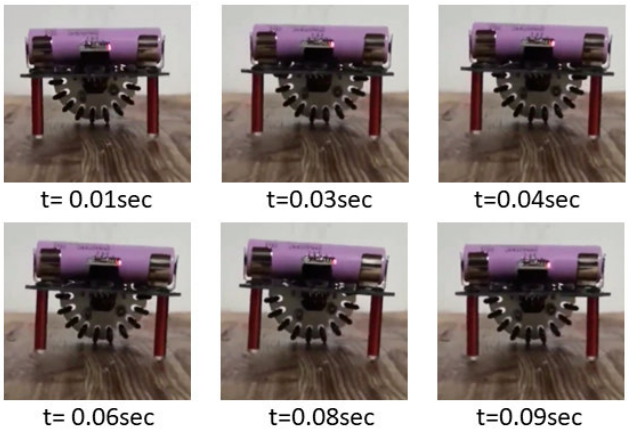


**FIGURE 6.** A front view taken from a real experiment single step. The experiment was captured with a 960fps camera, from which the frames were extracted.

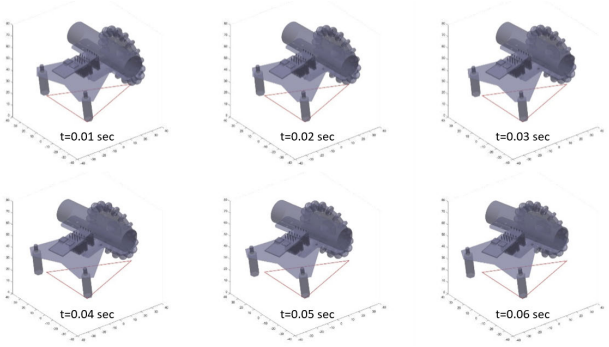


**FIGURE 7.** A perspective view of the simulated gait over 0.05 seconds. The wheel's turn results with the robot pivoting around the leg (the right most).

It was observed that increasing the wheel acceleration leads to larger rotation around the $\widehat{b}$ axis and faster, larger rotations around the $\widehat{z}$ axis. In other words, higher acceleration results in the robot taking bigger ''steps'', leading to faster progress. However, it was also noted that with higher accelerations, the robot may deviate more abruptly from the desired path.

To assess the robot's ability to accurately follow a straight path, a specific experiment was conducted. The robot was positioned on a flat surface and instructed to move in a straight line. Using image analysis, the robot's position was recorded every 1 second for a total duration of 40 seconds. This experiment was repeated 10 times.

Figure 10 illustrates the trajectories of the robot's movement during each of these ten experiments.

After completing 400 steps, a spread in the y-axis is observed, characterized by a standard deviation of $\sigma = 30mm$. This suggests that the standard deviation for a single step, denoted as $\sigma_y$, is approximately $0.27mm$. In contrast, the x-axis displays a mean deviation of $\mu_x = 350/400mm = 0.875mm$ per step, which explains the distribution of trajectories around the solid line depicted in Figure 10.

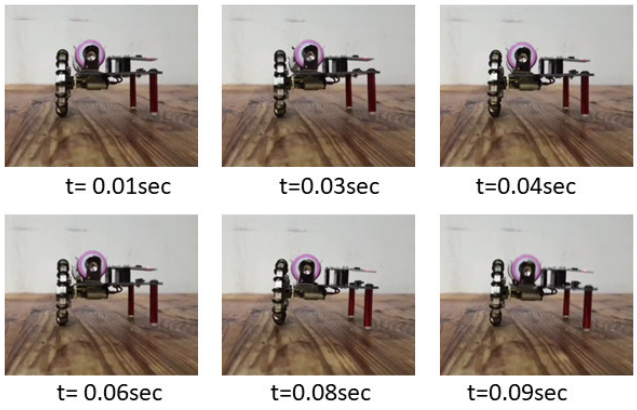


**FIGURE 8.** A single step: side view.

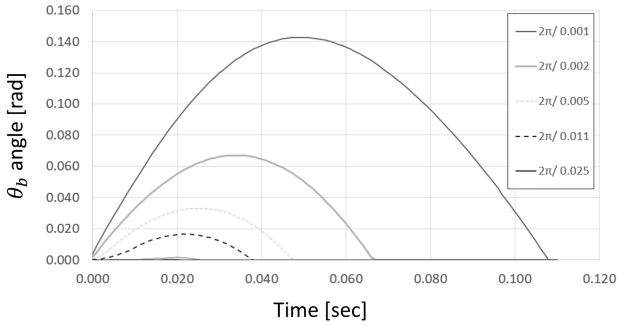


**FIGURE 9.** The body angle $\theta_b$ over a single step for different motor accelerations.

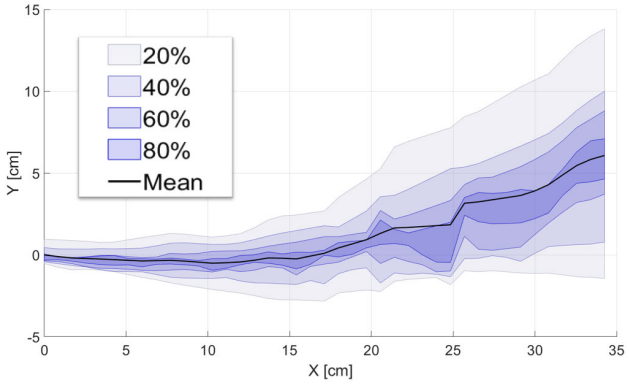


**FIGURE 10.** A fanchart of the robot's trajectories on the plane. Colors correspond to the trajectories' percentiles 20%-80%, the solid line represents the trajectories' mean value.

## V. DISCUSSION

The experimental results of our study on the robotic design presented both advantages and disadvantages. Firstly, the robustness of the design was demonstrated through the fabrication of 10 identical robotic units, all of which showed consistent, repeatable results.

Secondly, the simplicity of the design is a notable advantage, with only a single moving part and the requirement of only a single LiPo cell, eliminating the need for an

additional Battery Management System. The robot is capable of rotating about its own axis and can also achieve turning while in motion, with a non-zero turning radius, adding to its maneuverability.

Our experiments demonstrate the robot's remarkable ability to bear a load up to five times its own weight. The robot employs a dynamic mode of traversal, which involves sequentially lifting each leg. While this method proves effective in movement, it inherently results in a reduced traversal speed, particularly noticeable when the robot is carrying additional weight.

One of the experiment's objectives was to evaluate the precision of a robot's movement along a straight line (e.g. the x-axis), focusing on maintaining a straight trajectory. Figure 10 illustrates the walking behavior of a specific robot. Despite programming the robot to travel exclusively in the x-direction for a distance of 35 cm, an average deviation of 5 cm in the y-axis was observed (the reported linear motion was, in reality, executed as a curved trajectory with a curvature radius of 1250mm). This tendency leftward bias can be traced back to assembly flaws, including issues like uniform leg length and asymmetric motor actuation and they can be reduced by using asymmetrical sinusoidal motor rotation. While such deviations may be undesirable in precision navigation scenarios, they can be easily controlled using external position sensors like cameras or mitigated using odometry sensors such as optical flow, which we shall not implement here (note however, that in the context of swarm robotics, these deviations can be beneficial, as randomness contributes to emergent behaviors [3]).

However, there are some drawbacks. The walking speed of the robot is relatively low compared to other single-motor designs, which might limit its applications. The robot offers a low range of speeds since its motion is dynamically based.

Another limitation is its moderate power consumption. The robot's operation results in a power consumption of 0.2W during stepping motion, which exceeds the N20 DC motor's nominal requirement of 0.1W for continuous revolution. This increased consumption arises from the frequent changes in angular velocity inherent in our stepping motion. Nonetheless, despite the higher power demand, this feature enables the robot's simple design and its capability for both stepping and turning maneuvers.

## VI. CONCLUSION

In conclusion, this paper presents a novel mechanism for the design of planar mobile robots that operates with a single actuator, deviating from the conventional approach that relies on two or three actuators. The proposed mechanism was optimized through a dynamic analysis derived from Euler-Lagrange equations, allowing for efficient control and motion of the robot.

The experiments conducted as part of this study successfully demonstrated the translation and rotation capabilities of the planar walking robot. These experiments showcased the feasibility and effectiveness of the single actuator mechanism in achieving desired locomotion tasks.

However, it is crucial to acknowledge that additional research and development are essential to fully understand the capabilities and limitations of this innovative mechanism. Future studies should concentrate on refining the design; for instance, incorporating striding legs that point upwards could aid the robot in scenarios where flipping is a risk, thereby enhancing its versatility across various terrains and conditions. Moreover, investigating alternative control strategies and evaluating the robot's performance in real-world scenarios will be vital in advancing its application and functionality.

## APPENDIX
## KINETIC ENERGY ANALYSIS

Let us now proceed with a detailed formal development of Eq. 8. The kinetic energy of a rigid body in a system of axes whose origin is point O, where O is a stationary point, is calculated as follows:

$$E_k = \frac{1}{2}\omega^T I_O \omega$$

The kinetic energy of a rigid body when a system of axes is located at the center of mass is calculated as follows:

$$E_k = \frac{1}{2} m v_c^T v_c + \frac{1}{2}\omega^T I_c \omega$$

The kinetic energy of the MonoBot will be calculated as a superposition of the energy of the robot's body due to its rotational movement $\bar{\omega}_b$ around the point O and of the wheel energy due to its rotational $\bar{\omega}_w$ and linear $\bar{v}_w$ movement of its center of mass, here R is the rotation matrix which rotates $I_O$, the MonoBot's inertia tensor at steady state:

$$\begin{aligned} E_k &= \frac{1}{2}\bar{\omega}_b^T R^T I_O R \bar{\omega}_b + \frac{1}{2} m_w v_w^T v_w + \frac{1}{2}\bar{\omega}_w^T I_w \bar{\omega}_w \\ &= \frac{1}{2}(R_z \hat{b}_0 \dot{\theta}_b - \hat{z}\frac{r}{h}\dot{\theta}_w)^T R^T I_O R (R_z \hat{b}_0 \dot{\theta}_b - \hat{z}\frac{r}{h}\dot{\theta}_w) \\ &\quad + \frac{1}{2} m_w (K R_z \hat{b} \dot{\theta}_w)^T (K R_z \hat{b} \dot{\theta}_w) \\ &\quad + \frac{1}{2}(\hat{w}_0 \dot{\theta}_w + \hat{b}_0 \dot{\theta}_b)^T I_w (\hat{w}_0 \dot{\theta}_w + \hat{b}_0 \dot{\theta}_b) \end{aligned}$$

where

$$K = \begin{bmatrix} 0 & \frac{hr}{\ell^2} & 0 \\ -\frac{hr}{\ell^2} & 0 & 0 \\ 0 & 0 & 0 \end{bmatrix},$$

see Eq.6

$$\begin{aligned} &= \frac{1}{2}\dot{\theta}_b^2 \hat{b}_0^T R_z^T R^T I_O R R_z \hat{b}_0 - \dot{\theta}_b \dot{\theta}_w \frac{r}{h}\hat{z}^T R^T I_O R R_z \hat{b}_0 \\ &\quad + \frac{1}{2}\dot{\theta}_w^2 \left(\frac{r^2}{h^2}\right) \hat{z}^T R^T I_O R \hat{z} + \frac{1}{2}\dot{\theta}_w^2 m_w \hat{b}^T R_z^T K^T K R_z \hat{b} \\ &\quad + \frac{1}{2}\dot{\theta}_w^2 \hat{w}_0^T I_w \hat{w}_0 + \dot{\theta}_b \dot{\theta}_w \hat{b}_0^T I_w \hat{w}_0 + \frac{1}{2}\dot{\theta}_b^2 \hat{b}_0^T I_w \hat{b}_0 \end{aligned}$$

This sums up to the form (see Eq.8):

$$E_k = \frac{1}{2}\dot{\theta}_b^2 I_1 + \dot{\theta}_b\dot{\theta}_w I_2 + \frac{1}{2}\dot{\theta}_w^2 I_3 \tag{11}$$

where:

$$I_1 = \widehat{b}_0^\top R_z^\top R^\top I_O R R_z \widehat{b}_0 + \widehat{b}_0^\top I_w \widehat{b}_0$$

$$I_2 = \widehat{b}_0^\top I_w \widehat{w}_0 - \frac{hr}{\ell^2}\widehat{z}^\top R^\top I_O R R_z \widehat{b}_0$$

$$I_3 = \frac{h^2 r^2}{\ell^4}\widehat{z}^\top R^\top I_O R \widehat{z} + m_w \vec{b}^\top R_z^\top K^\top K R_z \vec{b} + \widehat{w}_0^\top I_w \widehat{w}_0$$

## REFERENCES

[1] O. Medina, A. Shapiro, and N. Shvalb, "Kinematics for an actuated flexible n-Manifold," *J. Mech. Robot.*, vol. 8, no. 2, Apr. 2016, Art. no. 021009.
[2] O. Medina, A. Taitz, B. B. Moshe, and N. Shvalb, "C-space compression for robots motion planning," *Int. J. Adv. Robotic Syst.*, vol. 10, no. 1, p. 6, Jan. 2013.
[3] O. M. N. Shvalb and S. Hacohen, "Statistical robotics: Controlling multi robot systems using statistical-physics," Tech. Rep. 0704, Duke University, Durham, NC, USA, 2023.
[4] S. H. Collins, M. Wisse, and A. Ruina, "A three-dimensional passive-dynamic walking robot with two legs and knees," *Int. J. Robot. Res.*, vol. 20, no. 7, pp. 607–615, Jul. 2001.
[5] X.-Z. Lai, J.-H. She, S. X. Yang, and M. Wu, "Stability analysis and control law design for acrobots," in *Proc. IEEE Int. Conf. Robot. Autom.*, May 2006, pp. 745–750.
[6] T. A. Mcmahon and G. C. Cheng, "The mechanics of running: How does stiffness couple with speed?" *J. Biomechanics*, vol. 23, pp. 65–78, Jan. 1990.
[7] Y. Aoustin and A. Formalskii, "Upward jump of a biped," *Int. J. Humanoid Robot.*, vol. 10, no. 4, Dec. 2013, Art. no. 1350032.
[8] C. D. Bellicoso, F. Jenelten, C. Gehring, and M. Hutter, "Dynamic locomotion through online nonlinear motion optimization for quadrupedal robots," *IEEE Robot. Autom. Lett.*, vol. 3, no. 3, pp. 2261–2268, Jul. 2018.
[9] N. Heess, D. Tb, S. Sriram, J. Lemmon, J. Merel, G. Wayne, Y. Tassa, T. Erez, Z. Wang, S. M. Ali Eslami, M. Riedmiller, and D. Silver, "Emergence of locomotion behaviours in rich environments," 2017, *arXiv:1707.02286*.
[10] A. Barjau and J. A. Batlle, "Predicting impact scenarios of a rimless wheel: A geometrical approach," *Nonlinear Dyn.*, vol. 110, no. 4, pp. 3209–3227, Dec. 2022.
[11] W. Znegui, H. Gritli, and S. Belghith, "Control of the compass-gait Walker using an enhanced poincaré map and via LMI-based optimization," in *Proc. 18th Int. Multi-Conf. Syst., Signals Devices (SSD)*, Mar. 2021, pp. 172–178.
[12] Y. Zheng, L. Li, F. Asano, C. Yan, X. Zhao, and H. Chen, "Modeling and analysis of tensegrity robot for passive dynamic walking," in *Proc. IEEE/RSJ Int. Conf. Intell. Robots Syst. (IROS)*, Sep. 2021, pp. 2479–2484.
[13] L.-W. Wang, K.-K. Song, F. Zhao, W.-L. Du, and X.-J. Wang, "Design of the single leg of the quadruped bionic robot with jumping," in *Proc. 3rd Annu. Int. Conf. Mech. Mech. Eng. (MME)*, 2017, pp. 603–608.
[14] Y. Zhang and V. Arakelian, "Design and synthesis of single-actuator walking robots via coupling of linkages," *Frontiers Mech. Eng.*, vol. 6, Jan. 2021, Art. no. 609340.
[15] D. Zarrouk and R. S. Fearing, "Controlled in-plane locomotion of a hexapod using a single actuator," *IEEE Trans. Robot.*, vol. 31, no. 1, pp. 157–167, Feb. 2015.
[16] S. Ito, S. Sugiura, Y. Masuda, S. Nohara, and R. Morita, "Mechanism and control of a one-actuator mobile robot incorporating a torque limiter," *J. Intell. Robotic Syst.*, vol. 97, no. 2, pp. 431–448, Feb. 2020.
[17] H. H. Hariri, G. S. Soh, S. Foong, and K. L. Wood, "A highly manoeuvrable and untethered under-actuated legged piezoelectric miniature robot," in *Proc. 43rd Mech. Robot. Conf.*, Aug. 2019.
[18] A. M. Hoover, S. Burden, X.-Y. Fu, S. Shankar Sastry, and R. S. Fearing, "Bio-inspired design and dynamic maneuverability of a minimally actuated six-legged robot," in *Proc. 3rd IEEE RAS EMBS Int. Conf. Biomed. Robot. Biomechatronics*, Sep. 2010, pp. 869–876.
[19] V. Böhm and K. Zimmermann, "Vibration-driven mobile robots based on single actuated tensegrity structures," in *Proc. IEEE Int. Conf. Robot. Autom.*, May 2013, pp. 5475–5480.
[20] O. M. U. Lax, N. Shvalb. (2023). *Monobot Showcase*. [Online]. Available: https://youtu.be/X6nEgkVpTzI

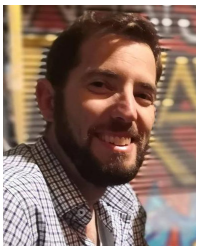

**URIYA LAX** is currently pursuing the degree with the Department of Mechanical Engineering, Ariel University, Israel. His research interest includes under-actuated robotic mechanical systems.

**ODED MEDINA** received the Ph.D. degree from Ben Gurion University. He is currently a Lecturer with the Department of Mechanical Engineering, Ariel University. In his research laboratory, he deals with motion planning problems and general computational problems in robotics, such as configuration space representation and minimal actuation problems of redundant robots. Amongst his early research projects are a real-time motion planner for hyper redundant serial robot aimed for pole climbing tasks. He also investigates the motion of hyper-redundant flexible mechanisms, which due to their flexibility require a large number of actuators. Most projects also included the designing and fabrication of actual mechanisms.

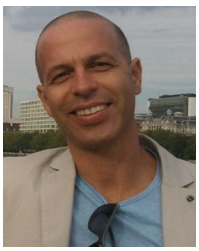

**NIR SHVALB** is currently an Associate Professor with the Faculty of Engineering and the Vice Dean of Ariel University, Israel. He heads the Robotics Research Laboratory. His main research interests include medical robotics, global path planning, and theoretical foundations of robotics. He is the Founder of several robotics startup companies amongst are Momentis Surgical and W Endoluminal Robotics.